Korean Journal of Remote Sensing, Vol.38, No.4, 2022, pp.365~374
https://doi.org/10.7780/kjrs.2022.38.4.4

ISSN 1225-6161 (Print)
ISSN 2287-9307 (Online)

Article

Activity of the Fushun West Open-pit Mine in China Observed by Sentinel-1 InSAR Coherence Images

Da-woon Jung [1] · **Hoonyol Lee** [2]†

Abstract: Mining activity causes environmental pollution and geological hazards such as ground subsidence or landslide of which continuous monitoring is necessary. In this study, the activity on the Fushun West Open-Pit Mine (FWOPM), one of the largest open-pit coal mines in Asia located in Fushun, Liaoning Province, China, was analyzed by using a time-series Sentinel-1 InSAR coherence dataset. By using the difference between the two Digital Elevation Models (DEM) of the area, it was possible to confirm that there was a stockpiling activity in the western area of the FWOPM while excavation activity in the eastern area. By using RGB composite images using the yearly-averaged InSAR coherence images, the activity of the mine was confirmed by period, which was confirmed by Google Earth optical images. As a result, it was possible to confirm three landslides and the related activities on the northwest slope and the dumping activity on the west slope of FWOPM.

Key Words: Sentinel-1, InSAR coherence, Fushun west open-pit mine, Landslide

1. Introduction

Mines are an essential source of raw materials for the industrial economy. Mining activities cause serious problems such as ground subsidence, landslides, and other geological hazards. In particular, landslides can cause sudden casualties and property damage. Therefore, continuous monitoring is essential to prevent environmental pollution and geological hazards in the mine areas. Remote sensing can explore an area where field surveys are limited and can detect changes in a wide area, enabling various observations depending on the purpose. The recent increase in freely accessible satellite data enabled us to monitor those hazards continuously. Especially, SAR systems can acquire homogeneous images regardless of weather conditions, day and night, which are suitable for surface change detection.

The types of mines are largely divided into open-pit mines and underground mines. In open-pit mines, logging and removal of topsoil are carried out before mining activity. It is easy to observe surface changes

Received August 2, 2022; Revised August 11, 2022; Accepted August 13, 2022; Published online August 23, 2022

[1] Master Student, Department of Geophysics, Kangwon National University, Chuncheon, Republic of Korea
[2] Professor, Department of Geophysics, Kangwon National University, Chuncheon, Republic of Korea

† Corresponding Author: Hoonyol Lee (hoonyol@kangwon.ac.kr)

due to mining activities or building construction. Therefore, using the InSAR coherence technique that detects the phase stability between two SAR images acquired at different times, effective observation of open pit mines is possible (Moon and Lee, 2019).

Fushun West Open-Pit mine (FWOPM) is located in Fushun, Liaoning Province, China (Qi *et al*., 2021). FWOPM was once the largest open-pit coal mine in Asia and operated from 1901 to 2018 (Zhou *et al*., 2011). The mine became very deep due to long-term mining and slopes have reached technical limitations. More than 90 landslides were reported inside the FWOPM before 2011 (Zhou *et al*., 2011). Most landslides occurred on the southern and northern slopes of FWOPM. More than 60% of landslides were concentrated during the rainy season (Zhou *et al*., 2011; Li *et al*., 2022). A series of examples include a landslide on the northern slope in 2012 (Li *et al*., 2015) and just above the area in 2016 (Sun *et al*., 2022).

In this study, two Digital Elevation Models (DEMs) were subtracted to identify the mining and dumping activities in FWOPM between 2000 to 2015. RGB composite image from the yearly-averaged Sentinel-1 InSAR coherence images was then used to analyze the activity of FWOPM such as landslides and mining activities from October 2016 to May 2020.

2. Study Area and Data

1) Study Area

Fushun coal mine is located in the Fushun Basin, NE China. Fushun city was well known as 'the capital of coal' for being rich in coal reserves. It has long been linked to the Chinese coal industry with a history of more than 100 years of coal mining (Dong *et al*., 2009; Zhou *et al*., 2011). FWOPM, the largest open-pit mine in Asia with an area of 10 square kilometers and a maximum depth of 400 meters, is located west of two open-pit mines in Fushun and operated from 1901 to

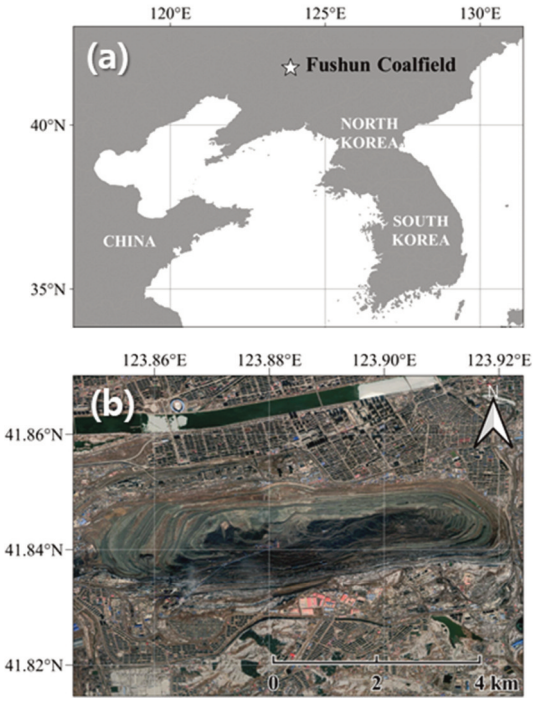

Fig. 1. The study area. (a) The location of Fushun city and (b) an overview of FWOPM.

2018 (Hu *et al*., 2017; Liu *et al*., 2022). The study area is affected by the East Asia monsoon. About 75% of the annual rainfall is concentrated in the rainy season from July to September (Nie *et al*., 2015). Long-term mining caused frequent landslides and subsidence due to the clay minerals contained in the greenish mudstone (Lu *et al*., 2022). This mine has been closed since 2018 and massive restoration works are in progress to change this hazardous area into an environmentally friendly site.

2) Data

The Sentinel-1 mission is composed of two satellites, Sentinel-1A and Sentinel-1B, sharing the same orbits. The revisit cycle of each satellite is 12 days. If both satellites are used, the revisit cycle can be shortened to 6 days. However, only the Sentinel-1B descending pass images were used in this study because the ascending pass did not have image acquisition regularly. The SAR scenes used for this study are summarized in Table 1.

Table 1. SAR scenes used in this study

Satellite	Sentinel-1 (C-band)
Data type	Single Look Complex (SLC)
Acquisition mode	Interferometric wide swath (IW)
Pass direction	Descending
Temporal coverage	07 October 2016–07 May 2020
Relative orbit (path)	105
Number of scenes	105

We also used two of the global DEM, The SRTM 1 Sec HGT DEM and Copernicus 30 m DEM, in data processing and getting elevation changes map. The SRTM 1 Sec HGT DEM is from the Shuttle Radar Topography Mission (SRTM) that used two radar antennas of the C-band and X-band system to acquire InSAR DEM during the 11-day flight from February 11, 2000 (Farr *et al*., 2007). It sampled from 60° north to 56° south latitude with a grid size of 1 arc-second (approximately 30 m × 30 m). The Copernicus DEM is based on the TanDEM-X Mission which was acquired between December 2010 and January 2015 and provided in three different versions: EEA-10, GLO-30, and GLO-90 (Fahrland *et al*., 2020). The Copernicus 30 m DEM is equivalent to GLO-30 data and has a latitude grid of 1 arc-second.

3. Methods

1) InSAR Data Processing

We used SeNtinel Application Platform (SNAP) software for data processing to generate InSAR coherence images. The study area was extracted from the entire image by selecting the corresponding bursts only. Accurate orbit data was also put to reduce the error. Then, the two SLC images were co-registered into the master and slave data respectively with the shortest time interval of 12 days from the dataset. As a result, 100 interferograms of 12 days intervals were obtained. The phase difference due to the earth's curvature and topographic phase was removed using

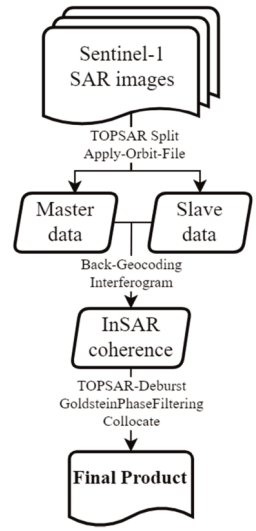

Fig. 2. Flow chart of Data processing.

SRTM 1 Sec HGT DEM to obtain interferograms and coherence images. In addition, filtering was performed by applying the nonlinear adaptive algorithm by Goldstein and Werner (1998).

2) Elevation Change

Subtracting the two DEMs acquired at different times, we can calculate the change in altitude during the intervening period. In this study, to investigate the activity inside the FWOPM before the study period, two global DEMs were used to check the altitude change that occurred in the study area between the SRTM 1 Sec HGT DEM and Copernicus 30 m DEM. In addition, we can also calculate the volume change from the elevation changes.

3) InSAR Coherence

SAR images record the intensity of backscattering from the ground in the form of a complex number. A complex correlation coefficient of two complex SAR signals (μ_1, μ_2) acquired at a time interval can be defined as follows (Lee, 2001).

$$\gamma = \frac{E[\mu_1, \mu_2^*]}{\sqrt{E[\mu_1, \mu_1^*]E[\mu_2, \mu_2^*]}} \quad (1)$$

where E[ ] is the mathematical expectation value, and * is the complex conjugate number. The coherence (ρ) is the amplitude of the complex correlation (Lee, 2001).

$$\rho = |\gamma| \quad (2)$$

InSAR coherence is a measure of signal stability and detects random surface changes occurring on the surface. A stable surface such as buildings and rocks has the value of coherence close to 1 while unstable targets such as trees and water converge to 0 (Moon and Lee, 2019).

As FWOPM is a coal mine with a soft surface, coherence values are affected severely by weather conditions such as snow and rain. It has a low coherence value throughout the coherence image due to precipitation events (Ferretti *et al*., 2007). Out of a total of 100 InSAR pairs, we only used 73 images for the analysis while the rest 27 images mostly in the rainy season were excluded due to their low coherence values in the study area.

4) RGB Composite of Averaged InSAR Coherence Images

Firstly, the activity for the entire period was viewed by producing an average coherence image for the entire period. Excluding 31 InSAR data with low coherence values, a total of 73 coherence images with a time interval of 12 days were used for the analysis in this study. The entire study period was then divided into three periods to produce average coherence images for each period. To check the activity analysis for each period at a glance, three averaged coherence images were put into the RGB channel to obtain an RGB composite image so that 2019 data (including early 2020) were set for the Red channel, 2018 data for Green, and 2017 data (including late 2016) for Blue. The meaning of each color in the RGB composite image produced using the averaged coherence image for each period can be explained by the pseudo-color theory (Fig. 3).

4. Results and Discussion

1) Elevation Change during 2010 and 2015

With the result of the elevation change using two global DEMs, it was confirmed that the altitude from 2000 to 2015 decreased in the eastern part and increased in the western part of the mine. Therefore, between 2000 and 2015, it was determined that mining was carried out in about 133,625,875 m^3 in the eastern part, and waste rock was deposited in about 167,189,594 m^3 in the western part. The stability of the slope in the waste rock fields would be lower than that in the mining area. Landslides would be more liable due to dumping activities in the waste rock field area on the west slope.

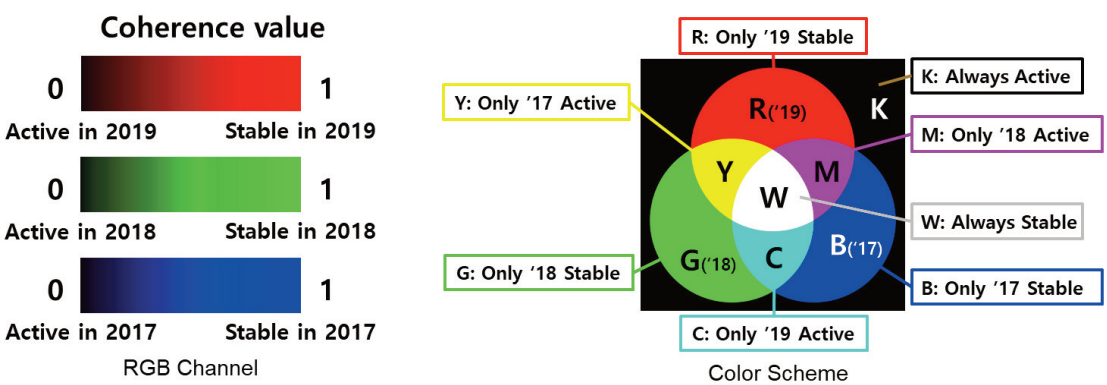

Fig. 3. A pseudo-color scheme of surface activity by the RGB composite of averaged InSAR coherence images by period (modified from Moon and Lee, 2021).

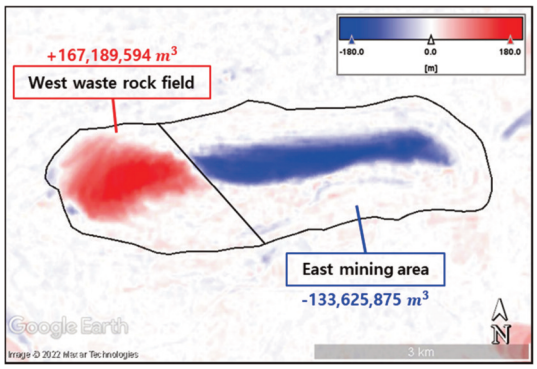

Fig. 4. Elevation and volume change in FWOPM during 2000 and 2015.

2) InSAR Coherence during Late 2016 and Early 2020

A total of 73 coherence images were obtained during the entire period of study. Firstly, to understand the overall mining activity during the study period, a total average coherence image was produced (Fig. 5(a)). By averaging several coherence images, it was possible to obtain the effect of correcting random errors in each image. In addition, to analyze the mining activity by period, the total period was divided into three periods and average coherence images were produced for each period (Fig. 5(b), (c), (d)). It was confirmed that the activity was concentrated on the northwest slope of the mine during the study area.

3) RGB Composite of Yearly-averaged InSAR Coherence Images

To check the yearly activities at a glance on the west and northwest slope, RGB composite image was produced by inputting annually averaged coherence images into R (2019), G (2018), and B (2017) channels, respectively. Various colors appeared in the interior of

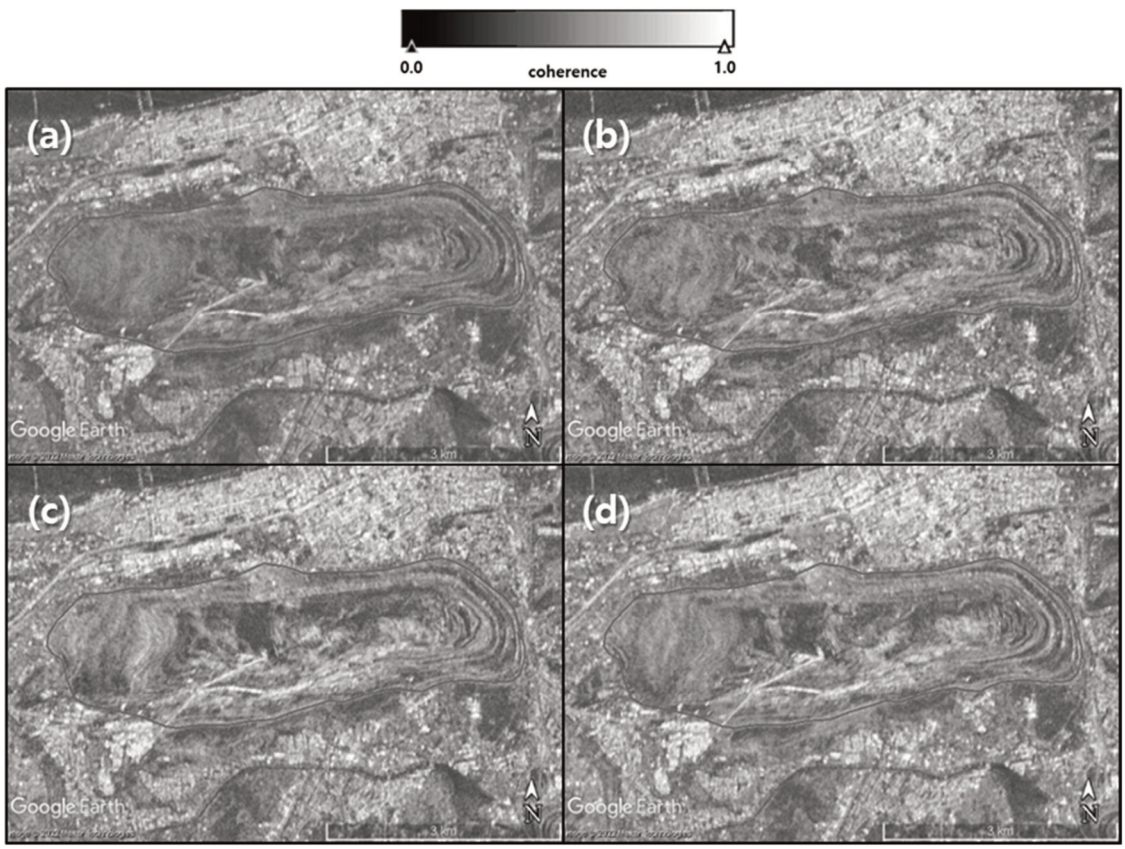

Fig. 5. Averaged InSAR coherence images. (a) Total average, (b) late 2016–2017, (c) 2018, and (d) 2019–early 2020.

the FWOPM as shown in Fig. 6. White areas indicate always high stability such as conveyors and buildings inside the mine. Various colors mean that there is a difference in activity by period. The black area, which means that it was always active, appeared mainly near the center of the northern slope. It was confirmed that the distribution of various colors appeared widely on the northwest slope right next to the black area and the west slope. Fig. 7 shows examples of time-series graphs of coherence values for various colors. In the next section, the changes due to the activity of the mines over periods were analyzed and compared with the optical images by projecting the RGB composite image on Google Earth.

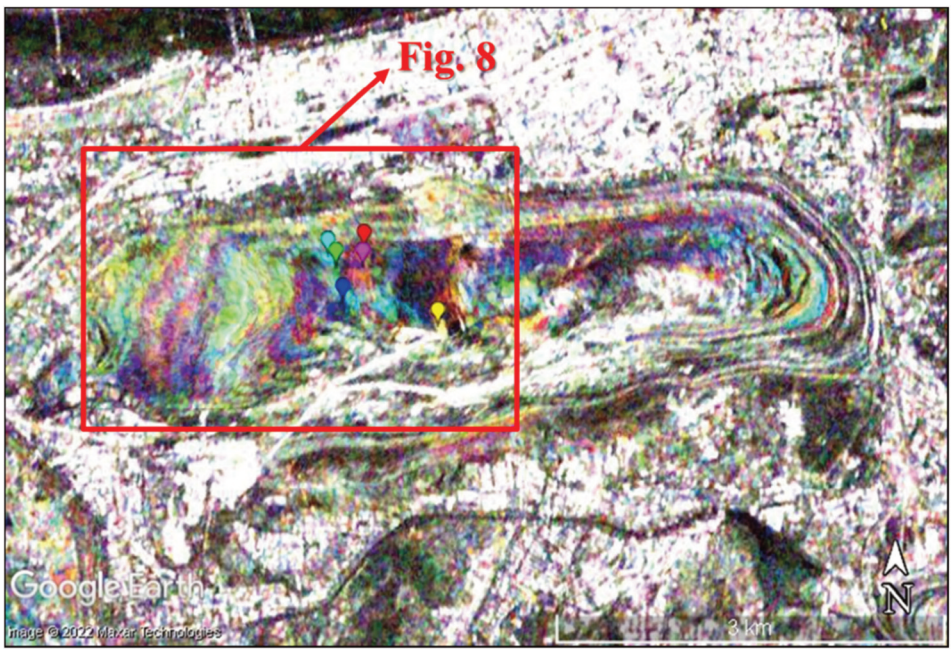

Fig. 6. RGB composite image from averaged coherence images by period (R: 2019–early 2020, G: 2018, B: late 2016–2017).

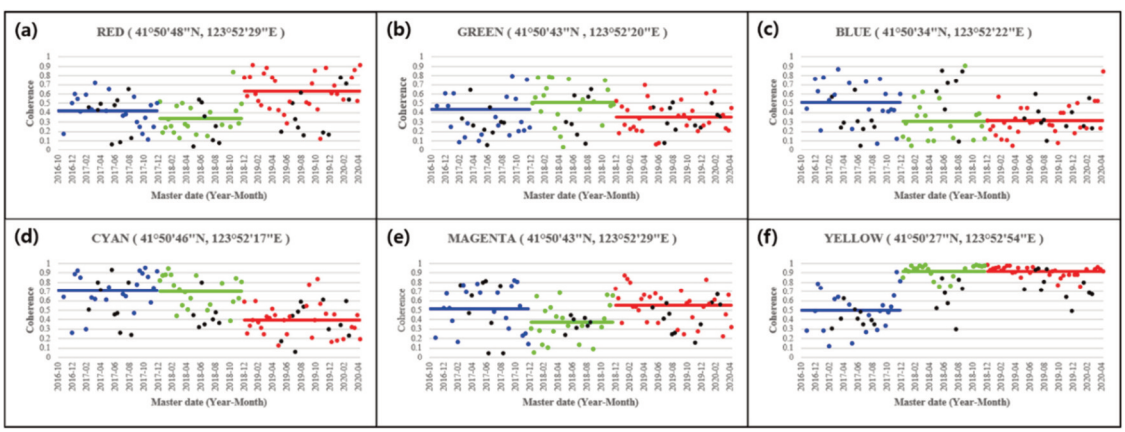

Fig. 7. The examples of 12-day coherence values in each pointed color pixel of Fig. 6. (a) Red, (b) Green, (c) Blue, (d) Cyan, (e) Magenta, and (f) Yellow. The dots shown in the graph indicate the coherence values of each data and the color indicates corresponding to each period (R: 2019, G: 2018, B: 2017). The black dots indicate coherence values excluded from averaging and the solid line indicates the averaged value of each period.

4) Landslides and Dumping Activities of FWOPM

(1) Landslides on the Northwest Slope in 2014 and 2016

In the optical image acquired on May 27, 2014 (Fig. 8(a)), we found an area of the landslide on the northern slope, which was an extension of the landslide in 2012 as mentioned in Li *et al*. (2015). It was confirmed in the optical images that it occurred in early 2014. We call it L1 (Landslide 1) with an area of about 0.1 km^2. The dumping equipment was filling up the step-shaped benches on the west slope. Another larger landslide (we call it L2) occurred on July 26, 2016 (Sun *et al*., 2022), as shown in the optical image of November 17, 2016 (Fig. 8(b)). The area of the L2 is about 0.48 km^2. The area located at the top of this landslide has been restored as shown in the optical image in Fig. 8(c). The RGB composite image (Fig. 8(e)) shows yellow color for the restored area, which means it was active in 2017 only and became stable afterward due to the completion of the restoration.

(2) A Landslide on the Northwest Slope in 2017

Looking at the optical image taken on August 29, 2017 (Fig. 8(c)), it was confirmed that a new landslide (we call it L3) with an area of 0.32 km^2 occurred on the northwest slope. To confirm the activity of the western half of FWOPM, we tried to examine the cause of color distribution due to activity in RGB coherence images by comparing it with high-resolution optical images by time provided by Google Earth.

This landslide occurred on a bench-type waste rock field. The landslide material washed away most of the benches, except for a small fraction of areas that maintained the shape of some benches inside L3 (Fig. 8(c)). Looking at the location of the dumping equipment in the L3 part of Fig. 8(c) and (d), it can be seen that the boundary of the northwest slope extends toward the center of the mine. It can also be seen that the red and magenta, meaning recent stability, are distributed in the right region of L3, and the cyan and green, meaning recent activity, are distributed in the left region of L3 (Fig. 8(e)). Therefore, it is considered that the stability of the collapsed northwest slope has been reinforced again by dumping activities from east to west after L3 occurred and until early 2020.

It is worth noting that it is difficult to estimate the exact day of occurrence of this landslide with the research method used in this study. This is because the annually averaged coherence images were input to the RGB channel in this study. In addition, landslides in FWOPM with a soft surface occur during the rainy season when the coherence value is lowered throughout the mine, making it more difficult to specify the timing of the landslide.

(3) Dumping Activity on the West Slope

As mentioned above, the appearance of band-shaped various colors on the west slope in the RGB composite image, Fig. 8(e), is considered to be a waste rock dumping activity of the FWOPM. Looking at the optical images in Fig. 8(a), (b), (c), (d), as time goes by, the waste rock dumping activity on the west slope is progressing. In addition, it was confirmed that the locations of the dumping equipment on the benches at the same height that fills the slope are gradually extending to the east. The reason why the band-shaped various colors appear on the western slope is considered to be due to the method of extending the benches while maintaining the slope stability. In the RGB composite image of Fig. 8(e), it can be seen that various colors are distributed in a band shape on the western slope. In addition, it can be confirmed that several stripes of the same color exist in different positions. This is because the dumping activity on the western slope is performed simultaneously on several benches. The stripes showing the same color in different locations are considered to have been active at the same time.

The red, green, and blue colors mean that the area was stable only for a year in 2019, 2018, and 2017,

respectively. The yellow, magenta and cyan colors indicate that the area was actively dumped only in 2017, 2018, and 2019, respectively, and was stable otherwise (Fig. 8(e)).

5. Conclusions

In this study, we analyzed the activity of the northwest and west slope of FWOPM using InSAR coherence images and compared them with Google Earth optical images. As a result, it was possible to

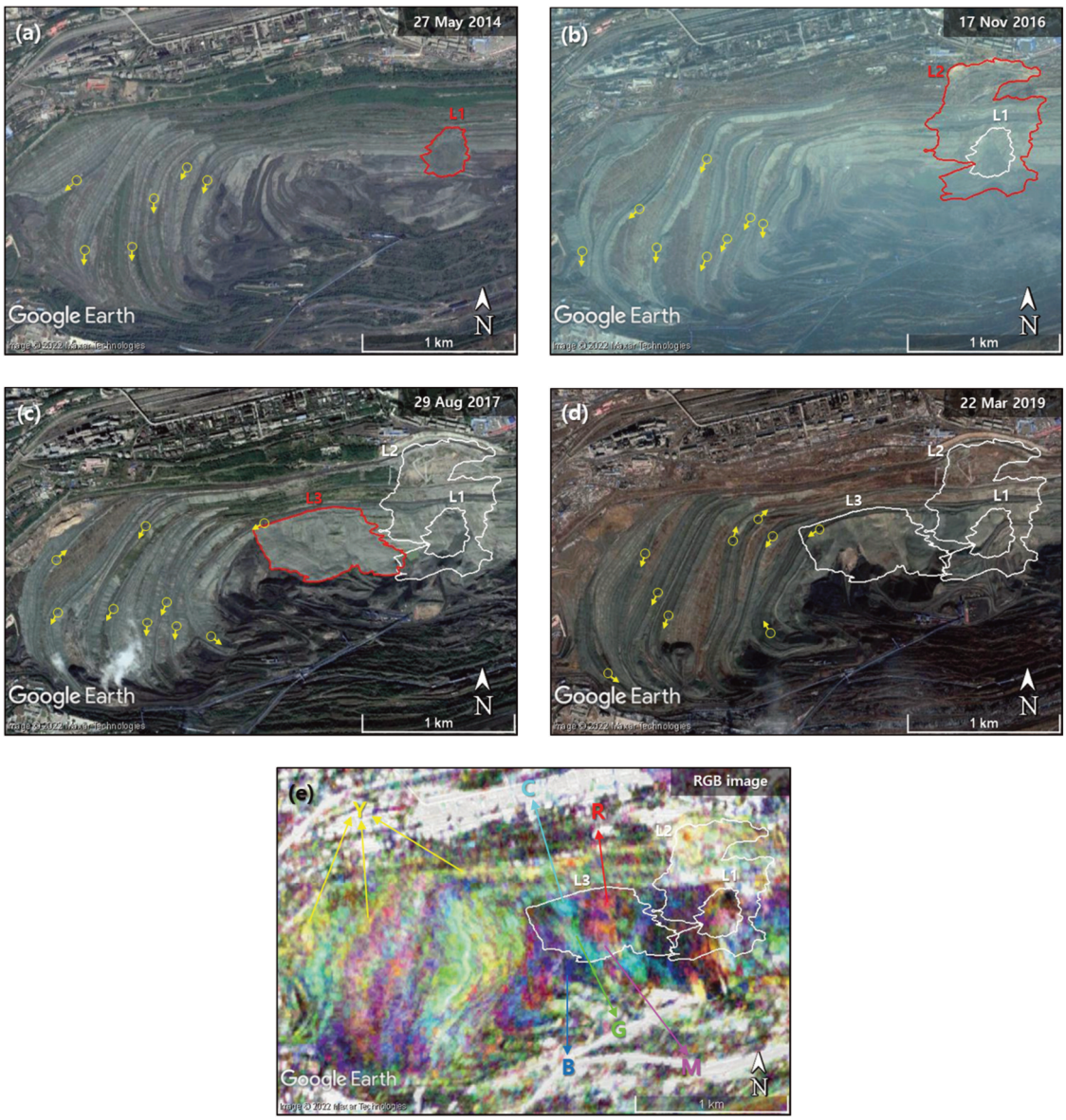

Fig. 8. Images of the northwest region of FWOPM. Google Earth images of (a) 27 May 2014, (b) 17 Nov 2016, (c) 29 Aug 2017, and (d) 22 Mar 2019. (e) RGB composite image of yearly averaged coherence images of R (2019), G (2018), and B (2017). The yellow circles and arrows indicate the location of the dumping equipment and its direction of movement. The red lines indicate the boundary of the landslide area newly found on that date while the white line indicates the previous landslide area.

discover another new landslide event in 2017 not documented in the previous studies and to confirm the activity that occurred during the recovery process. In addition, an analysis was also conducted on the western dumping area where extension activities on its benches occurred at different locations over time.

It was difficult to estimate the exact timing of the occurrence of the landslide in 2017 by analyzing the 12-day InSAR coherence values due to the soft surface of FWOPM that has too low coherence during the rainy season. More frequent observation with InSAR pairs is required for this purpose. In this case, RGB composite of InSAR coherence images with a shorter temporal baseline would detect the occurrence of landslides.

Acknowledgements

This research was supported by the Basic Research Project of Korea Institute of Geoscience and Mineral Resources (KIGAM) funded by the Ministry of Science and ICT of Korea, National Research Foundation of Korea (NRF-2022R1F1A1071054 and No. 2019R1A6 A1A03033167), and Ministry of the Interior and Safety as Human Resource Development Project in Disaster Management.

References

Dong, Y., B. Fu, and Y. Ninomiya, 2009. Geomorphological changes associated with underground coal mining in the Fushun area, northeast China revealed by multitemporal satellite remote sensing data, *International Journal of Remote Sensing*, 30(18): 4767-4784. https://doi.org/10.1080/01431160802662923

Fahrland, E., P. Jacob, H. Schrader, and H. Kahabka, 2020. Copernicus DEM Product Handbook, https://spacedata.copernicus.eu/documents/20126/0/GEO1988-CopernicusDEM-SPE-002_ProductHandbook_I1.00.pdf, Accessed on Jun. 25, 2020.

Farr, T.G., P.A. Rosen, E. Caro, R. Crippen, R. Duren, S. Hensley, M. Kobrick, M. Paller, E. Rodriguez, L. Roth, D. Seal, S. Shaffer, J. Shimada, J. Umland, M. Werner, M. Oskin, D. Burbank, and D. Alsdorf, 2007. The shuttle radar topography mission, *Reviews of Geophysics*, 45(2): 1-33. https://doi.org/10.1029/2005RG000183

Ferretti, A., A.V. Monti-Guarnieri, C.M. Prati, F. Rocca, and D. Massonnet, 2007. *INSAR Principles B*, ESA publications, Noordwijk, Netherlands.

Goldstein, R.M. and C.L. Werner, 1998. Radar interferogram filtering for geophysical applications, *Geophysical Research Letters*, 25(21): 4035-4038. https://doi.org/10.1029/1998GL900033

Hu, W., L. Wu, W. Zhang, B. Liu, and J. Xu, 2017. Ground Deformation Detection using China's ZY-3 Stereo Imagery in an Opencast Mining Area, *ISPRS International Journal of Geo-Information*, 6(11): 361. https://doi.org/10.3390/ijgi6110361

Lee, H., 2001. *Interferometric synthetic aperture radar coherence imagery for land surface change detection*, Huxley School, Imperial College, London, UK.

Li, Q., D. Song, C. Yuan, and W. Nie, 2022. An image recognition method for the deformation area of open-pit rock slopes under variable rainfall, *Measurement*, 188: 110544. https://doi.org/10.1016/j.measurement.2021.110544

Li, Z., L. Li, L. Wang, and R.Y. Liang, 2015. A case study integrating numerical simulation and GB-InSAR monitoring to analyze flexural toppling of an anti-dip slope in Fushun open pit, *Engineering Geology*, 197: 20-32. https://doi.org/10.1016/j.enggeo.2015.08.012

Liu, C., Y. Cui, C. Chen, J. Lyu, B. Li, and L. Wang,

2022. Research on the south side landslide at west open-pit coal mine in Fushun City, Liaoning Province of China, *Geological Bulletin of China*, 41(5): 713-726 (in Chinese with English abstract). https://doi.org/10.12097/j.issn.1671-2552.2022.05.001

Lu, J., T. Xu, X. Tang, M.J. Heap, J. Xu, T. Yang, and X. Zhao, 2022. Nanoindentation-based characterization of micromechanical properties of greenish mudstone from deep Fushun West open-pit mine (Fushun city, China). *Geomechanics and Geophysics for Geo-Energy and Geo-Resources*, 8(2): 1-20. https://doi.org/10.1007/s40948-022-00371-9

Moon, J. and H. Lee, 2019. Analysis of Open-Pit Mining Activities Using Sentinel-1A/B Coherence Imagery, *Proc. of 2019 Asian Conference on Remote Sensing (ACRS)*, Daejeon, South Korea, Oct. 14-18, vol. 1, pp. 2446-2453.

Moon, J. and H. Lee, 2021. Analysis of Activity in an Open-Pit Mine by Using InSAR Coherence-Based Normalized Difference Activity Index, *Remote Sensing*, 13(9): 1861. https://doi.org/10.3390/rs13091861

Moon, J., G. Kim, and H. Lee, 2021. Surface Change Detection in the March 5 Youth Mine Using Sentinel-1 Interferometric SAR Coherence Imagery, *Korean Journal of Remote Sensing*, 37(3): 531-542 (in Korean with English abstract). https://doi.org/10.7780/kjrs.2021.37.3.13

Nie, L., Z. Li, M. Zhang, and L. Xu, 2015. Deformation characteristics and mechanism of the landslide in West Open-Pit Mine, Fushun, China, *Arabian Journal of Geosciences*, 8(7): 4457-4468. https://doi.org/10.1007/s12517-014-1560-2

Qi, Y.N., S.B. Liao, and Q.L. Wang, 2021. Research on evaluation of mining area ecological security based on GF-1 satellite imagery—taking Fushun West open-pit mine for example, *IOP Conference Series: Earth and Environmental Science*, 783(1): 012128. https://doi.org/10.1088/1755-1315/783/1/012128

Sun, S.W., L. Liu, J.B. Hu, and H. Ding, 2022. Failure characteristics and mechanism of a rain-triggered landslide in the northern longwall of Fushun west open pit, China, *Landslides*, 1-20. https://doi.org/10.1007/s10346-022-01926-3

Zhou, J.J., L. Chen, Z.L. Fu, and K.K. Xie, 2011. Study on geological hazards and countermeasures in Fushun mining area, *Applied Mechanics and Materials*, 71: 4839-4843. https://doi.org/10.4028/www.scientific.net/AMM.71-78.4839